Appendix G–End Region Design Models

Table of Contents

List of Figures

List of Tables

G.1 Confinement Reinforcement Design Model

The 2007 AASHTO LRFD Bridge Design Specifications contain prescriptive requirements for the quantity and placement of confinement reinforcement located in the bottom flange of pretensioned concrete I-girders. This chapter proposes a rational model that can be used to design confinement reinforcement as an alternative to the prescriptive requirements of AASHTO LRFD. The model considers a wide range of conditions and variations, yet is intended to be practical enough for use by bridge design engineers. Variables in the design model include: flange and bearing geometry, strand size and placement, effective prestress force, concrete and steel material properties, and the effects of steel bearing plates. Derivation of the model is presented, and the model is compared to experimental results from the published literature.

The proposed design model can be used to calculate the quantity of confinement reinforcement required to prevent lateral-splitting failure at ultimate load. The model is formulated to capture the multitude of variables that exist in pretensioned girders, but be practical enough for use by bridge designers. The model does not consider the function of confinement reinforcement in controlling cracks during prestress transfer. This topic, however, is covered in section G.2.

Experimental and analytical work from the previous chapters has shown that confinement reinforcement carries transverse tension forces due to prestressing and applied loads. By carrying these forces the confinement reinforcement functions to prevent lateral-splitting failure and provides a normal force whereby strand tension forces can be transferred to the concrete once strut-and-tie behavior has initiated. The ultimate strength design model considers both of these functions. Forces generated due to these functions are referred to as the transverse tie force (F_{TT}), and the strand anchorage force (F_{SA}).

Strand anchorage and transverse tie functions of confinement reinforcement are analogous to the local zone and general zone reinforcement in post-tensioned (PT) structures. Figure 1 shows the manner in which the anchorage zone in a post-tensioned (PT) structure is partitioned into local and general zones. The local zone is a highly stressed region that resides immediately under the anchorage device and requires significant confinement reinforcement to prevent bursting stresses from causing localized failure. It is within the local zone that PT forces

are transferred to the concrete. The general zone in a PT structure is the area where PT forces are transmitted throughout the member.

Conceptually the end region of a pretensioned beam can be divided into a local and general zone (Figure 1). General zone size is comparable to that of a PT anchorage and can be designed by the same approach as is used for PT anchorage zones. Pretensioned local zones, however, are longer because force transfer occurs gradually throughout the transfer length rather than through an anchorage device. Large, very localized lateral bursting stresses that are present immediately under the anchorage in a PT local zone are thus avoided in pretensioned end regions.

In pretensioned local zones the concrete immediately surrounding a prestressing strand is subjected to radial stresses from the Hoyer effect, which is illustrated in Figure 2. The Hoyer effect occurs due to Poisson expansion of the strands in the lateral direction when the strands are cut at prestress transfer. The beneficial effect of this expansion is to generate sufficiently large frictional forces at the concrete-strand interface to transfer the prestressing force into the concrete. As illustrated in Figure 1 this has been shown to occur in a relatively uniform manner over the transfer length.

Confinement reinforcement is typically placed such that some bars support loads from both local and general zones. Accordingly, confinement force due to the transverse tie is also utilized as the force required for strand anchorage. The proposed design procedure calculates the load demand on confinement reinforcement as the larger of the local and general zone loads. Or in other words, the model calculates confinement reinforcement required for the greater of the strand anchorage or transverse tie force.

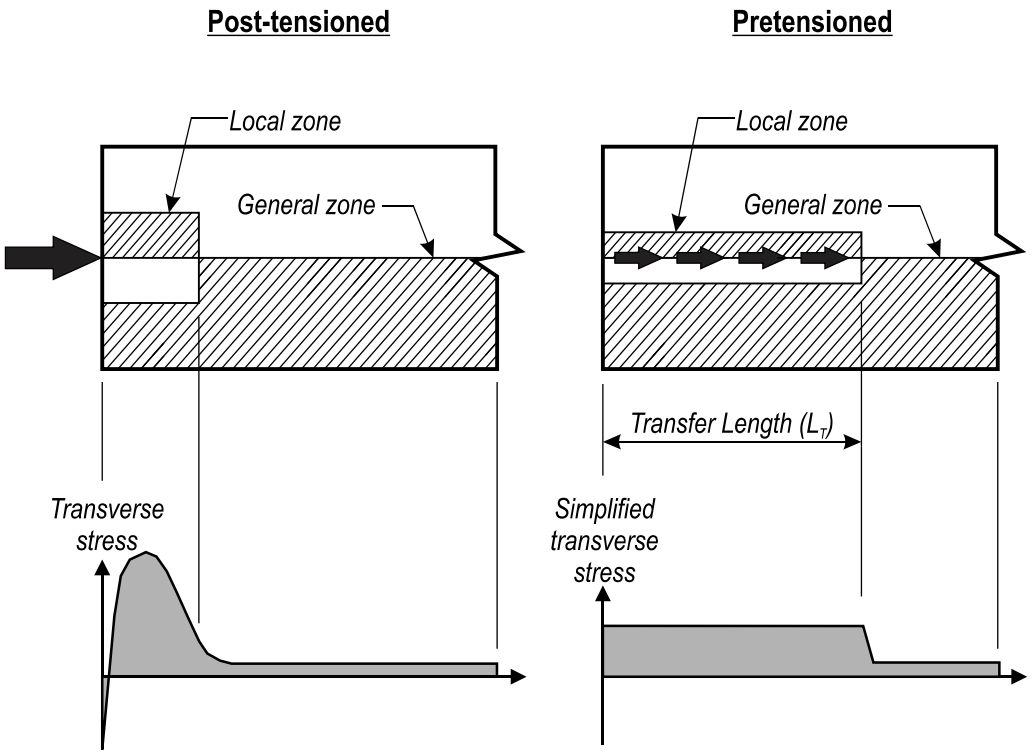

Figure 1–Local and general zones

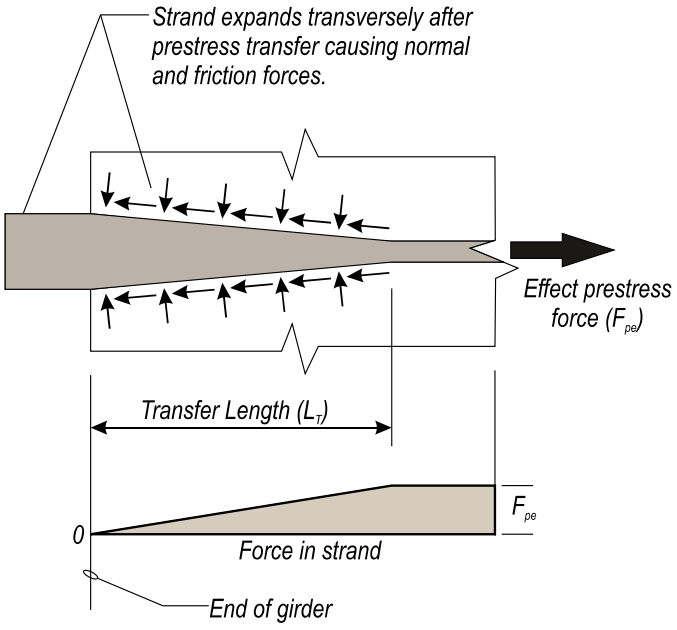

Figure 2–Illustration of transverse and frictional forces caused by the Hoyer effect

G.1.1 Model Derivation

G.1.1.1 Transverse Tie Force

Calculation of the transverse tie force is based on the strut-and-tie models shown in Figure 3. This figure describes transfer of the ultimate reaction (R_u) from the web, through the bottom flange and into the bearing pad. The struts and ties are symmetric about the z (vertical) axis.

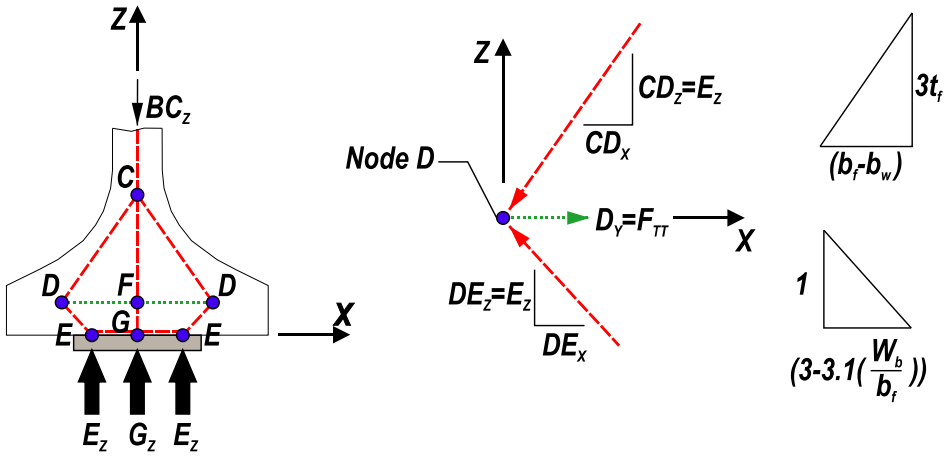

(a) Narrow Bearing

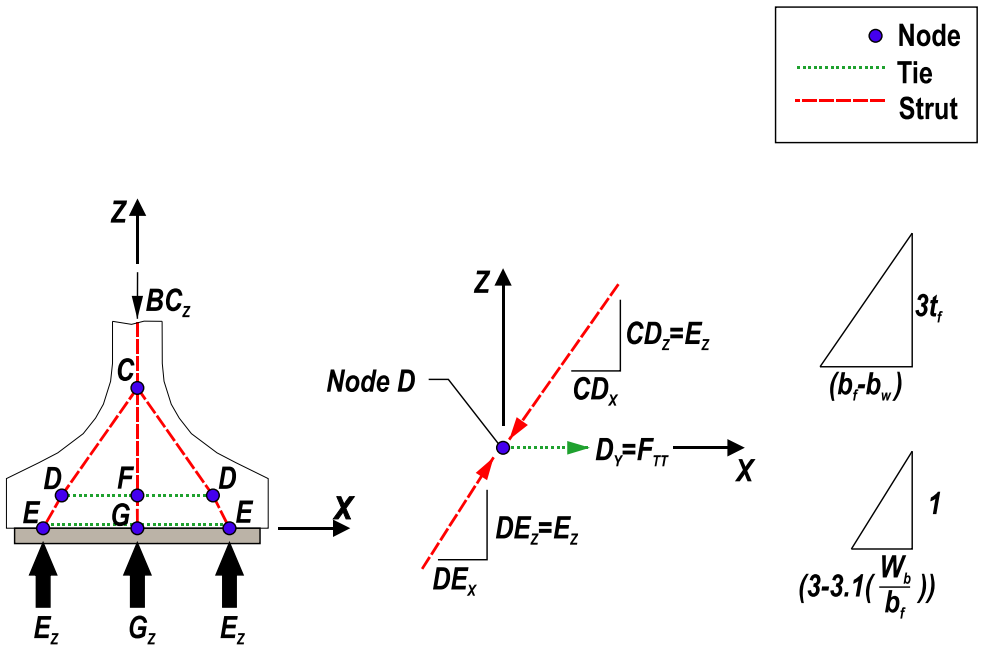

(b) Wide Bearing

Figure 3–Transverse tie force strut-and-tie models

Compressive force BC_Z equals the ultimate reaction and is carried to the support through three separate load paths. Force in each path is assumed to be proportional to the quantity of strands associated with that path; strands in the flange are assumed to connect to *D* nodes and strands below the web are assumed to connect to node *F*. Thus the vertical (z-direction) component of load traveling path *C-D-E* can be calculated by Equation 1-1:

$$CD_Z = DE_Z = E_Z = R_u\left(\frac{n_f}{n_{strand}}\right) \quad \text{1-1}$$

Where:

CD_Z = z-component of force in member *CD*

DE_Z = z-component of force in member *DE*

E_Z = Reaction at node *E*

R_u = Factored reaction force

n_f = number of strands in the flange

Using the strut and tie model shown in Figure 4a the slope of strut CD can be determined as follows:

$$Slope_{CD} = \frac{3t_f}{(b_f - b_w)} \quad \text{1-2}$$

Where:

t_f = Minimum thickness of bottom flange

b_f = Bottom flange width

b_w = Web width

Cross-sections from AASHTO, FDOT, Nebraska Department of Roads, and Washington State Department of Transportation were used to determine Equation 1-2. If exceptionally slender bottom flanges such as that shown in Figure 4b are used, then Equation 1-2 does not apply and the angle must be calculated directly.

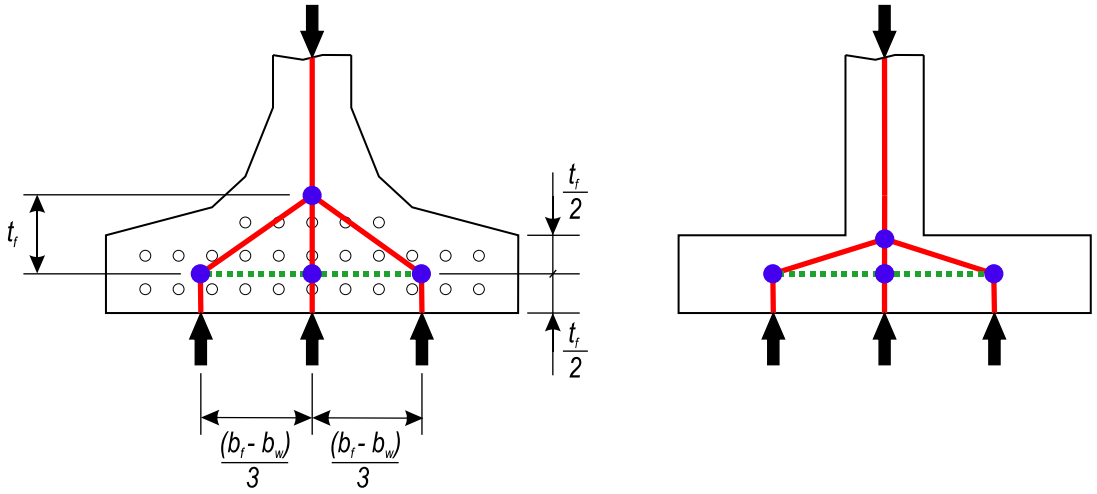

Figure 4–Node layout

Member *DE* slope can be calculated by Equation 1-3. When the bearing width is close to the flange width (Figure 3a), the slope calculated by Equation 1-3 is positive indicating that x-component of force in member *DE* acts in the positive x-direction. When the bearing width is smaller than the flange width (Figure 3b), the slope of member *DE* is negative, indicating that the x-component acts in the negative direction.

$$Slope_{DE} = \frac{1}{\left(3.1\left(\frac{W_b}{b_f}\right) - 3\right)} \qquad 1\text{-}3$$

Where:

W_b = Width of bearing

The horizontal (x-direction) force components in members *CD* and *DE* are calculated by Equations 1-4 and 1-5, respectively. These equations are derived from the vertical (z-direction) force component from Equation 1-1 and the slopes from Equations 1-2 and 1-3.

$$CD_X = R_u\left(\frac{n_f}{n_{strands}}\right)\left(\frac{(b_f - b_w)}{3t_f}\right) \qquad 1\text{-}4$$

$$DE_X = R_u\left(\frac{n_f}{n_{strands}}\right)\left(3.1\left(\frac{W_b}{b_f}\right) - 3\right) \qquad 1\text{-}5$$

The transverse tie force is equal to the force in member *DF*, and can be calculated from equilibrium in the x-direction at node *D*:

$$F_{TTu} = CD_X - DE_X \quad \text{1-6}$$

Substituting for CD_X and DE_X and simplifying, Equation 1-6 can be rewritten as:

$$F_{TTu} = R_u \left(\frac{n_f}{n_{strands}}\right)\left[\frac{(b_f - b_w)}{3t_f} - 3.1\left(\frac{W_b}{b_f}\right) + 3\right] \quad \text{1-7}$$

G.1.1.2 Strand Anchorage Force

Strand anchorage force refers to the normal force required to generate strand forces through friction. This force must be resisted by the concrete tensile strength, the confinement reinforcement, or both to ensure that the frictional force transfer between strands and concrete is maintained. If the concrete tensile strength and confinement are not sufficient bond is lost and the strand slips.

In addition to friction, force transfer between strands and concrete also occurs due to adhesion, mechanical interlock. Adhesion and mechanical interlock, however, are relatively small and are conservatively neglected. Also, it is thought unlikely that adhesion and mechanical interlock are significant at ultimate load after concrete around the strands has cracked.

At ultimate load it is assumed that internal forces in the end region can be described by strut-and-tie modeling as was done in calculating the transverse tie force. Strut-and-tie models conservatively neglect concrete tensile strength. This assumption will also be made in calculation of the strand anchorage force. Concrete around the strands will be assumed to have cracked and not be available to provide the normal force required to generate friction at the strand-concrete interface. In calculating the strand anchorage force, it is assumed that all of the normal force is supplied by confinement reinforcement.

Aknoukh (2010) presented a similar friction-based approach for designing confinement reinforcement. The Aknoukh model considered strand anchorage through on a horizontal section using a friction coefficient of 1.4. The proposed method is distinct from Aknoukh because it considers anchorage forces on vertical sections through the bottom flange, and because it uses a more conservative (and realistic) friction coefficient of 0.4. The proposed model is also distinct in that transverse tie forces are considered.

Equilibrium in the direction of the strand length requires that the total frictional force at the strand-concrete interface be equal and opposite of the effective prestress in the strand. The normal force required to generate the frictional force is equal to the frictional force divided by the friction coefficient at the strand-concrete interface. Based on this rationale, the normal force required to develop the effective prestress in an individual strand can be calculated by Equation 1-8:

$$F_N = \frac{A_{ps} f_{pe}}{\mu} \qquad 1\text{-}8$$

Where:

F_N = Normal force on an individual strand required to develop prestress

A_{ps} = Cross-sectional area of prestressing strands

f_{pe} = Effective prestress

μ = Coefficient of friction between concrete and strand, taken as 0.4

Although seven-wire strand does not have a circular cross section, it is believed that this simplification does not significantly affect the results of the strand anchorage force model. The same assumption was made by Oh et al (2006) in the development of a strand transfer length model. Using this assumption the Oh model correlated well with experimental data. The round strand assumption is also considered reasonable for the current model derivation.

Figure 5 illustrates the idealized normal stress acting on a single strand within the transfer length. The normal stress (f_N) can be calculated by assuming that the normal force (F_N) required to prevent strand slip is distributed evenly around the circumference and along the transfer length.

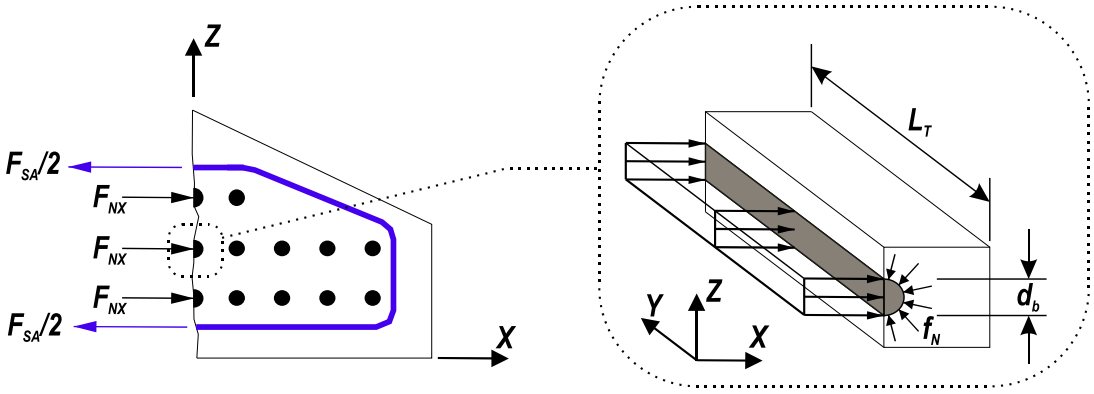

Figure 5–Strand anchorage force

The geometric properties of the strand can then be used to form equation1-9:

$$f_N = \frac{F_N}{d_p L_T \pi} \quad \text{1-9}$$

Where:

f_N = Normal stress at strand-concrete interface

d_p = Diameter of prestressing strand

Substituting Equation 1-8 into Equation 1-9 into gives:

$$f_N = \frac{A_{ps} f_{pe}}{d_p L_T \pi \mu} \quad \text{1-10}$$

The transverse (x-direction) component of the normal force on an individual strand can be calculated using a pressure vessel analogy by multiplying the stress in Equation 1-10 by the projected area of the strand over the transfer length:

$$F_{Nx} = f_N d_p L_T \quad \text{1-11}$$

Where:

F_{Nx} = Transverse normal force on an individual strand

Substituting Equation 1-10 into Equation 1-11 and simplifying gives:

$$F_{Nx} = \frac{A_{PS} f_{pe}}{\pi \mu} \quad \text{1-12}$$

The total x-direction force along an arbitrary section can be determined from the product of the transverse component and the number of strands along the section. This force is defined as the strand anchorage force and is given as:

$$F_{SA} = F_{NX} n_c = \frac{A_{ps} f_{pe} n_c}{\pi \mu} \quad \text{1-13}$$

Where:

F_{SA} = Strand anchorage force

n_c = Number of strands along critical section

Equation 1-13 can be used to calculate the strand anchorage force on any arbitrary section. The maximum strand anchorage force occurs through the section that intersects the maximum number of strands.

G.1.1.3 Quantity and Placement

Preceding sections have presented equations for calculating the transverse forces resisted by confinement reinforcement at ultimate load. The design force in the confinement reinforcement is equal to the greater of the transverse tie or strand anchorage forces:

$$F_{CRu} = \text{maximum } (F_{SA}, F_{TTu}) \qquad 1\text{-}14$$

Where:

F_{CRu} = Factored design force in confinement reinforcement

The reason for using the greater for the transverse tie or strand anchorage forces can be understood by considering the forces acting on a node in the bottom flange strut-and-tie model. For example, forcing acting on node D in Figure 3 come from struts in the concrete and ties in the reinforcement. In deriving the transverse tie force it was shown that the forces at node D are based on equilibrium and geometric properties. The same forces acting on node D are also the forces that generate the strand forces (acting in the y-direction at node D) through friction. Additional strand anchorage force is not required. Thus confinement reinforcement capacity need only be the greater of the strand anchorage force or the transverse tie force.

The quantity of confinement required at ultimate load is equal to the confinement reinforcement design load divided by the specified yield stress of the reinforcement:

$$A_{CR} = \frac{(F_{CRu})}{f_{yCR}} \qquad 1\text{-}15$$

Where:

A_{CR} = Required area of confinement reinforcement

f_{yCR} = Yield stress of confinement reinforcement

Data from the experimental program demonstrate that steel bearing plates contribute confinement to the bottom flange at ultimate load. To account for this, the proposed design model allows the bearing plate to replace up to 50% of the confinement required by Equation 1-15. The plate is not allowed to totally replace confinement reinforcement because the confining influence of the plate on its own was not enough to prevent lateral-splitting failure in

experiments. Bearing plates should not be considered as confinement reinforcement unless the bearing width and the spacing between plate anchorage points are *both* greater than 75% of the flange width. These requirements ensure that the bearing plate is in tension (Figure 3b), and is sufficiently anchored to provided confinement.

The confining effect of end diaphragms has also been shown to prevent splitting failures in experimental tests (Ross et al. 2011). End diaphragms, however, are not present during prestress transfer and therefore do not constitute a replacement for confinement reinforcement.

Results from the experimental program demonstrate that confinement reinforcement is most effective when placed near the end of the girder. As such, confinement reinforcement required by Equation 1-15 should be placed as close to the end of the girder as reasonable, but should also be placed over a distance of at least the transfer length.

G.1.2 Model Comparison with Experimental Results

In this section the proposed design model is evaluated against experimental data from 41 unique tests of pretensioned concrete girders reported in the literature (Appendix B, Appendix D, Llanos et al. 2009, Morcous et al. 2010, Tadros et al 2010, Deatherage et al 1994). Figure 6 compares confinement reinforcement installed in each test girder with the required confinement reinforcement calculated using the proposed model (Equation 1-15). The factored reaction force used to calculate the transverse tie force (F_{TT}) was taken as the nominal shear strength. Provided confinement reinforcement, plotted on the vertical axis, was taken as the area of confinement reinforcement placed within the transfer length. If present, the embedded steel bearing plate area was allowed to contribute up to 50% of the confinement requirement. Prestress losses were assumed to be 20 percent.

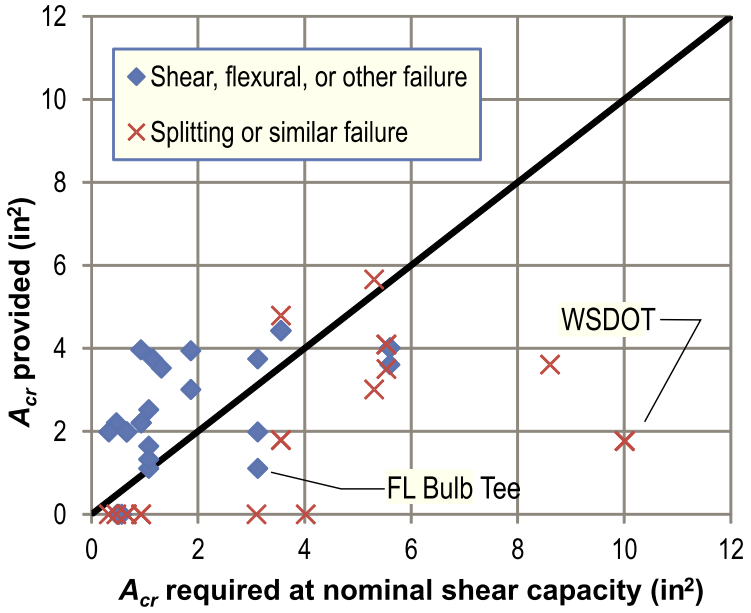

Figure 6–Design model compared to nominal strength of experimental girders

Points that fall below the solid line have less confinement than calculated by the model, and are predicted to fail due to splitting or lateral-bursting. The proposed model correctly identified all but two of the specimens that failed in lateral-splitting, bearing, or similar modes. Splitting and similar failures are denoted by the 'X' markers. The model incorrectly predicted failure in eight cases, as denoted by the diamond shaped markers that fall below the solid line. In most cases where the failure mode was not accurately predicted, the provided confinement reinforcement was within 1.5 in^2 of the calculated requirement, indicating a desirable degree of conservatism in the model.

The point marked "FL Bulb Tee" on Figure 6 shows the greatest level of disagreement with the proposed model. This data point represents a Florida Bulb Tee section (Tadros et al. 2010), which had only 35% of the calculated confinement reinforcement, but still did not fail due to lateral-splitting. Shear reinforcement in this specimen terminated in a hook at the bottom of the beam. Hook tails were placed under the strands, were oriented transverse to the axis of the beam, and extended to the edge of the bottom flange. Additional splitting resistance demonstrated by the specimen is attributed in-part to the confinement provided by these hook tails. Confining effects from hooks are neglected in the proposed model due to inadequate hook development. The Florida Bulb Tee was supported on a steel plate during testing. Splitting resistance of the specimen is also attributed to frictional force between the girder and plate.

Friction force at the bearing is thought to have had a greater impact on the bottom flange confinement than the hook tails from the vertical reinforcement.

The point label "WSDOT" on Figure 6 represents four tests of Washington wide flange girders (Tadros et al. 2010); each girder had identical calculated and provided confinement reinforcement. Numerous strands were located in the outer portion of the slender bottom flanges. During prestress transfer, it was observed that splitting cracks formed in the bottom flanges. Although not explicitly identified in the research, photographs of the failed beams suggest that lateral-splitting action occurred during testing.

The ultimate strength design model was also compared to the experimental data pool using the maximum shear force. For each data point, the maximum shear force reported in the literature was substituted into the model in lieu of the factored reaction force. As with the comparison at nominal shear capacity, the model also compares well with the maximum experimental shear forces (Figure 7). Points on the figure labeled "FL Bulb Tee" and "PC Bulb Tee" did not exhibit splitting failure in spite of having less confinement than calculated by the model. As with the FL Bulb Tee section discussed in Figure 6, the indicated specimens in Figure 7 were also supported on steel plates during testing. These plates were not embedded plates and were not considered in the model calculations; however they are thought to have provided additional splitting resistance to the FL and PC Bulb Tee specimens. This result indicates that the model may be conservative for girders that are supported on rigid surfaces such as steel plates or concrete bent caps.

Figure 8 shows the data set if the external steel bearing plates used in the tests were considered to provide confinement similar to embedded steel bearing plates. The external steel bearing plates were only considered if they were wide enough to provide confinement (Figure 3b). External steel bearing plates were not considered in specimens that also had embedded plates. Accuracy of the model in categorizing failure model improved when the external bearing plates were considered. All but one of the incorrectly categorized results was within 0.5 in^2 of the solid black line that denotes the border between failure modes.

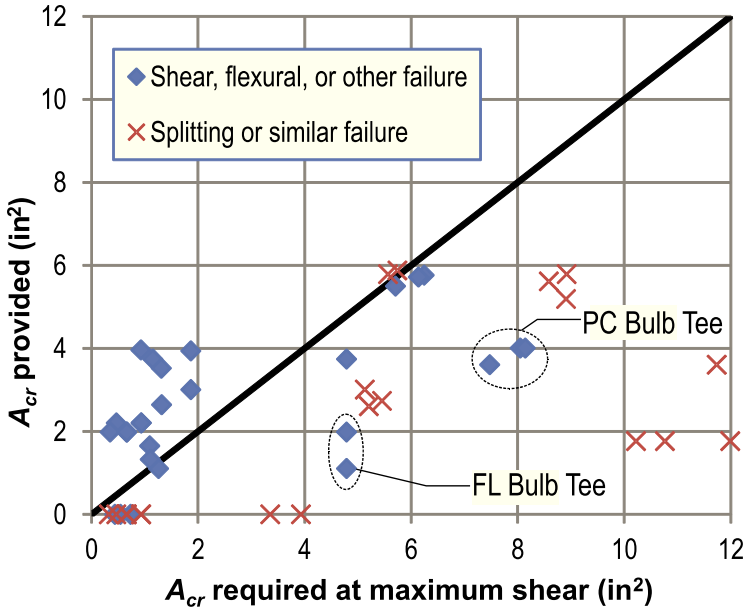

Figure 7–Design model compared to experimental girders at maximum shear

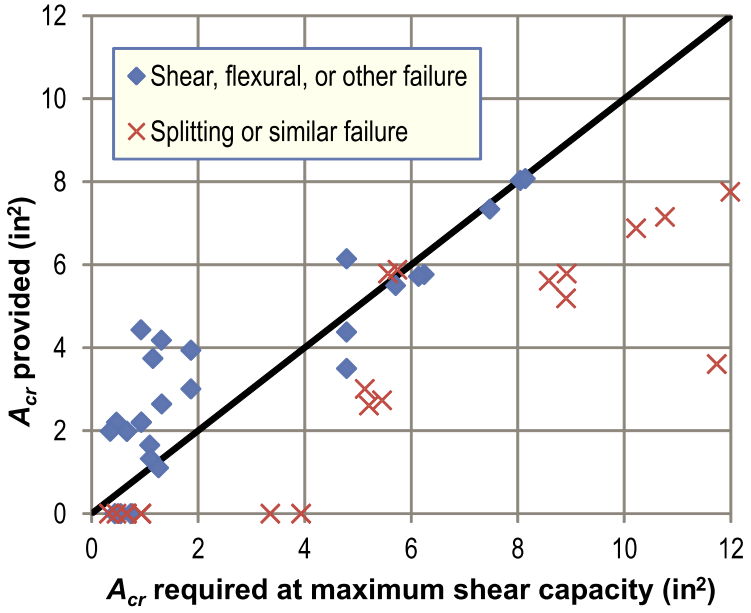

Figure 8–Design model compared to experimental girders at maximum shear (external bearing plates considered)

G.1.3 Ultimate Strength Design of Confinement Reinforcement

The ultimate strength model derived previously can be used for LRFD design using 1-16:

$$\phi A_{CR} f_{yCR} = F_{CRu} \quad \text{1-16}$$

Where:

A_{CR} = Required area of confinement reinforcement

f_{yCR} = Yield stress of confinement reinforcement

ϕ = Resistance factor

The required area of confinement reinforcement is such that the confinement reinforcement must provide a design strength greater than the force generated by the strand anchorage or the transverse tie. The resistance factor should be determined using the LRFD reliability analysis of the limit states. In lieu of this it is reasonable to treat this reinforcement the same as tension steel in an anchorage zone (ϕ = 1.0).

G.1.4 Summary and Conclusions

A rational design model was developed for designing confinement reinforcement at ultimate strength. The model considers strand anchorage and transverse tie requirements, which are analogous to local and general zone requirements in post-tensioned concrete members. The ultimate strength model was compared to 41 unique tests of pretensioned concrete girders reported in the literature. The model was found to have good agreement with the published test results. The model is recommended for the design of confinement reinforcement and bearing plates at ultimate load.

G.2 Serviceability Model

Experimental and analytical research presented in previous Appendices demonstrates that transverse tensile stress in the bottom flange of pretensioned I-girders can lead to flange splitting cracks during fabrication. It is believed that the following behaviors contribute to tensile stress and flange cracking:

- Hoyer effect
- Eccentric prestress forces
- Self-weight reaction

Flange splitting cracks can reduce the durability of concrete I-girders by allowing contaminates to enter the bottom flange and initiate corrosion of prestressing steel or chemical attack on the interior concrete. A serviceability design model is presented in this chapter for quantifying bottom flange splitting stress. The model is derived from a variety of sources including the work of other researchers, finite element modeling, and basic mechanics. Stress from the model can be compared to concrete tensile capacity to determine the likelihood of bottom flange splitting cracks.

Experimental and analytical research indicates that the largest transverse tensile stresses in the bottom flange occur at the member end. The majority of flange-splitting cracks in the experimental girders were located at or close to the specimen ends. Accordingly, the serviceability model provides equations for calculating the worst-case transverse tensile stress occurring at member ends. Calculated stresses at the member end can be compared to concrete tensile strength criteria to evaluate the likelihood of flange splitting cracks. Possible strength criteria are discussed later in this chapter.

In the final section of this chapter, experimental cracks data are compared to stresses calculated from the proposed model. The model and data are found to have a high degree of correlation.

G.2.1 Causes of Bottom Flange Splitting at Prestress Transfer

Flange splitting cracks in the bottom flange are caused by transverse splitting stresses that occur due to a combination of the Hoyer effect, eccentric prestress forces, and the self-weight reaction. The following sections describe the mechanics associated with of each of these effects.

G.2.1.1 Hoyer Effect

The diameter of a prestressing strand decreases during pretensioning due to the Poisson effect (Figure 9a and b). When tension is released during prestress transfer the strands expand towards their original diameter. Expansion is partially restrained by the surrounding concrete resulting in normal stresses and proportional frictional forces at the strand-concrete interface. This behavior was named for Ewald Hoyer, the German Engineer who first wrote of radial expansion of prestressing strands (Hoyer 1939).

Expansion of prestressing strands is greatest at the edge of the concrete where strand tension is zero after prestress transfer (Figure 9d). At locations beyond the transfer length the strand expansion is negligible because strand tension is nearly the same before and after release. Change in radial expansion is approximately linear between the concrete edge and the end of the transfer length (Oh et al. 2006). Consequently, radial and annular stresses in the concrete also vary linearly along the transfer length.

Variable expansion of the strands leads to a wedge-like shape after prestress transfer. This shape creates mechanical bond between strand and concrete. Additional bond improvement comes from the radial stresses at the interface, which allow the generation of frictional forces. Wedge action and frictional forces are thus beneficial consequences of the Hoyer effect because they enable the transfer of prestress forces. The Hoyer effect can also have detrimental consequences on the behavior and capacity of pretensioned girders. Concrete surrounding strands cracks when stresses due in-part to the Hoyer effect exceed concrete tensile capacity.

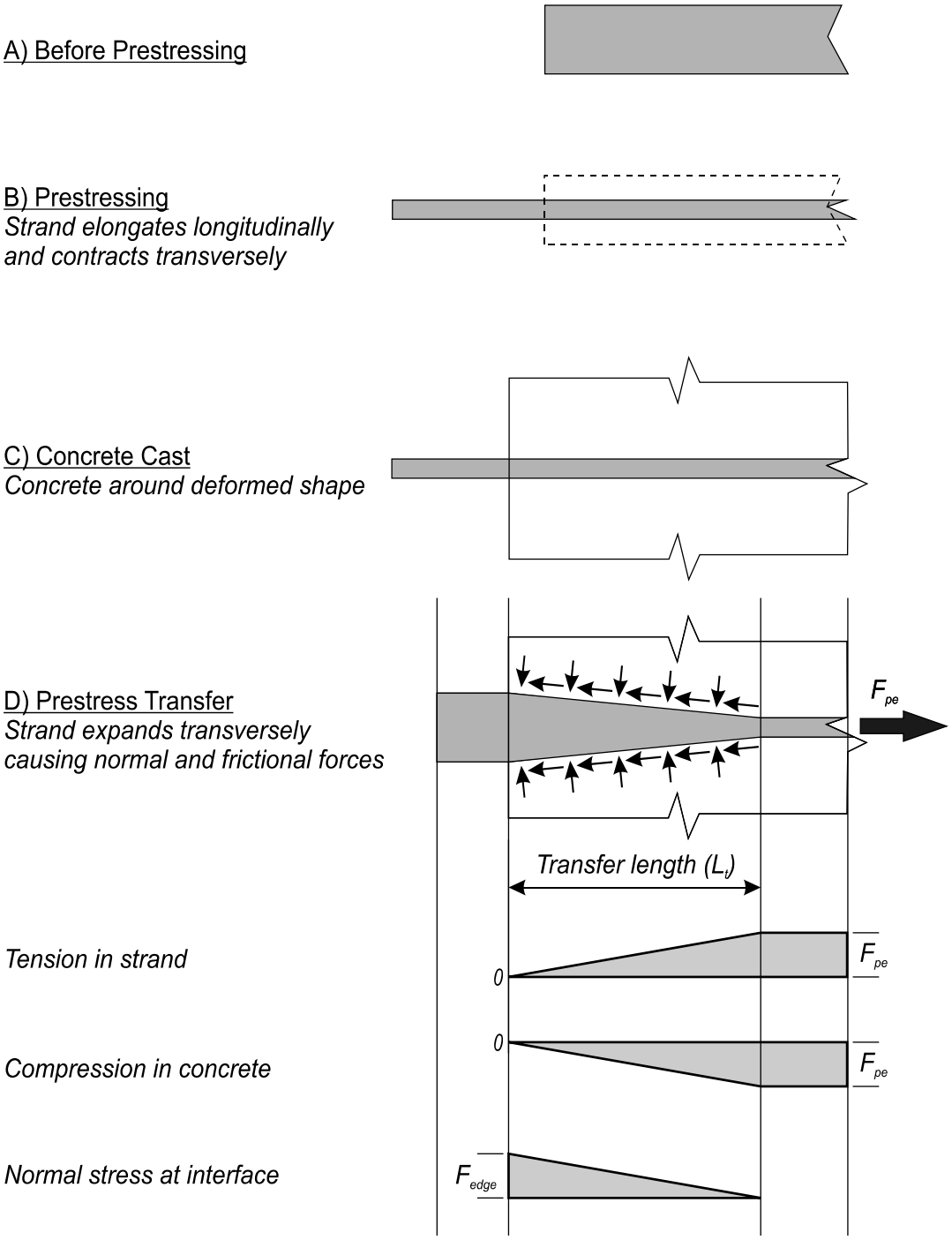

Figure 9–Hoyer effect A) strand before stressing, B) strand after prestressing, C) concrete cast around strand, and D) stresses and forces after transfer

G.2.1.2 Eccentric Prestress Forces

Tension forms in the bottom flange as prestressing forces from the outer strands are transferred to the concrete (Figure 10). This tension forms in response to the eccentricity

between prestressing forces from outer strands and the equal and opposite resultant force in the member. Tension is partially relieved as inner strands are released. This process has been demonstrated experimentally and analytically in previous chapters and is dependent on the strand bond pattern and strand cutting pattern. Tension stress due to eccentric prestress forces is referred to as "peeling" stress because they act to peel the outer portion of the bottom flange away from the web. Strands in the experimental program and in analytical models were cut from the outside-in. This detensioning pattern is assumed in the equations derived in this chapter.

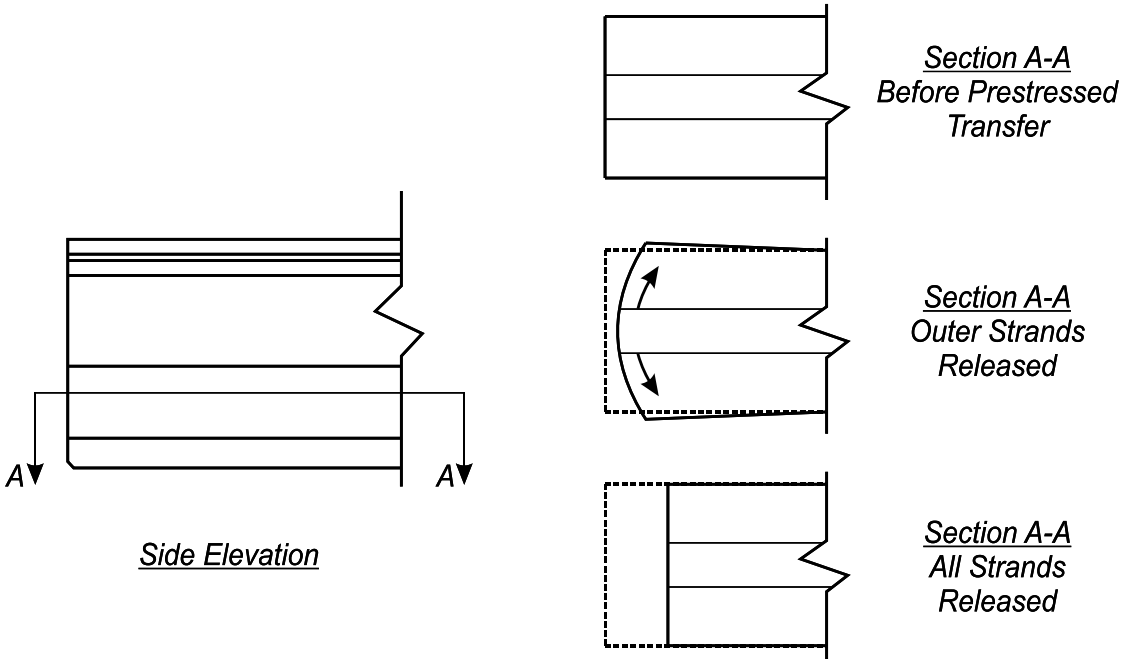

Figure 10–Flange tension due to outer strands

G.2.1.3 Self-Weight Reaction

Girders camber upward during prestress transfer after the prestressing moment exceeds the self-weight moment (Figure 11). After cambering, girders are supported by reactions at each end. Tensile stresses form in the bottom flange above the reaction points due to the flange bending illustrated in Figure 12.

Previous FE analyses show that self-weight reactions produce tensile and compressive transverse stresses in the FIB bottom flange (See Appendix F). Analysis also demonstrate that self-weight reaction stresses are small relative to peeling stresses, and that average stress on sections through the outer flange is near zero or slightly compressive. Because of this, self-

weight reaction stresses on sections through the outer portion of the FIB bottom flange are conservatively neglected in the proposed serviceability model. This assumption may not be reasonable for other cross-sections and for long-span FIB girders.

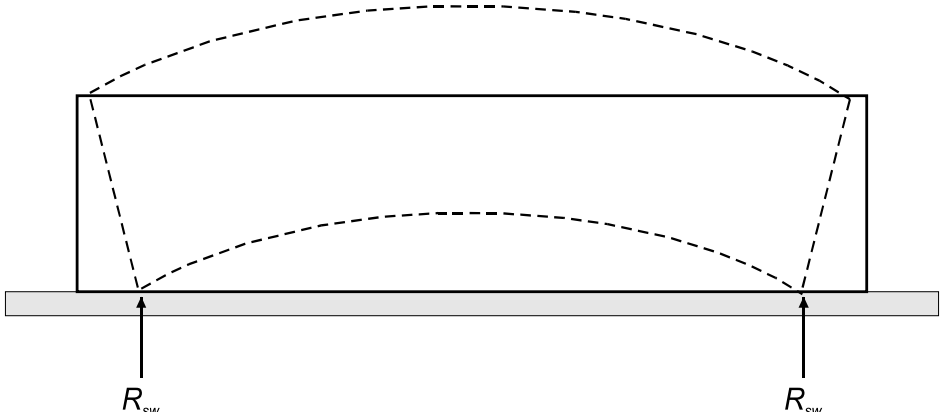

Figure 11–Camber due to prestress force

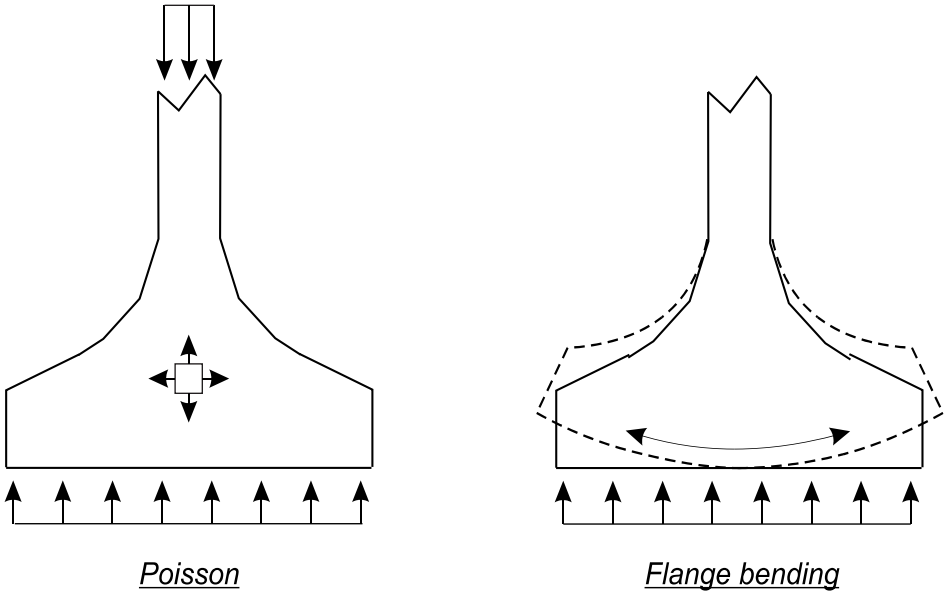

Figure 12–Self-weight reaction effects

G.2.2 Transverse Splitting Stress Model Derivation

Experimental results indicate that vertical splitting cracks can occur at multiple locations in the bottom flange (Figure 13). The proposed model focuses on splitting cracks through the

outer portion of the flange. Bottom flange splitting cracks below the web are not considered because they are associated with extreme strand bond patterns that are not permitted in FDOT production girders. Splitting cracks below the web were observed in the experimental program, but only in specimens with bonding patterns that placed fully bonded strands in the outer flange and shielded strands below the web.

An outside-in cut pattern is commonly used in FDOT production girders. As such, the serviceability model assumes an outside-in cut pattern. This pattern was used in construction of the experimental girders, as well as the FE models used to develop the serviceability model. The model does not apply to girders with other cut patterns.

Two critical conditions are considered in the design model:

- **Maximum Peeling**. Previous experimental and analytical research show that the maximum peeling stress along a given section occurs when only the outboard (closer to the outside edge) strands are cut (Figure 14). This condition is referred to as the "maximum peeling" condition.
- **Combined**. This condition occurs when strands along a given section are cut and Hoyer stresses are superimposed with peeling stress. It is referred to as the "combined" condition.

The model does not consider stress conditions when inboard (closer to the centerline) strands have been cut. Previous analytical work shows that cutting of inboard strands reduces peeling stresses on a given section.

Figure 13–Flange splitting in experimental girder.

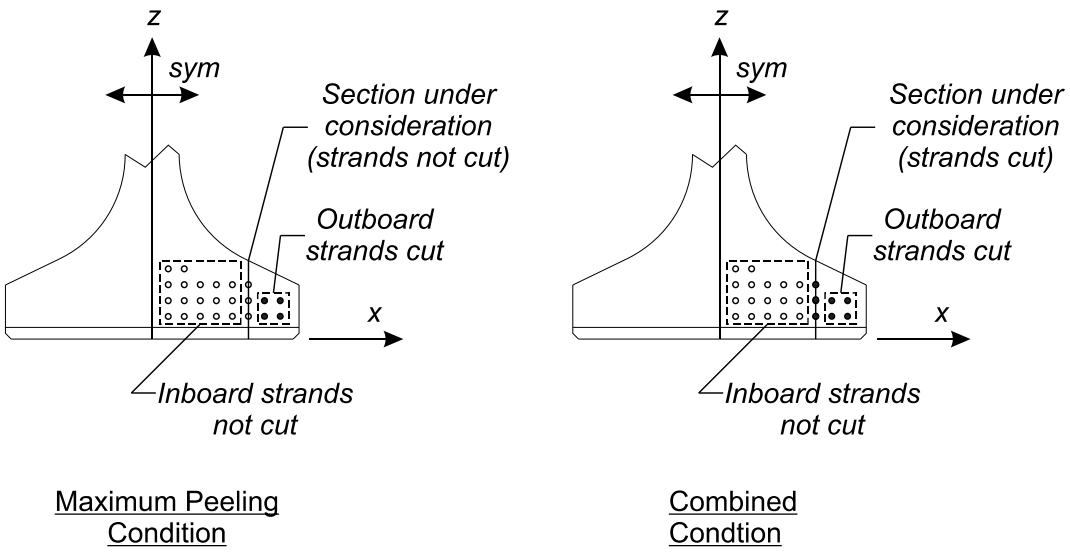

Figure 14–Strand cutting conditions

G.2.2.1 Hoyer Stress

Hoyer stress is calculated using a model developed by Oh et al. (2006). The Oh model is based on equilibrium, material constitutive properties, and strain compatibility. It assumes radial expansion of a steel cylinder surrounded by concrete (Figure 15). Equation 2-1 is for calculating radial stress at the steel-concrete interface. Figure 16 shows the radial stress distribution calculated from Equation 2-1 for a strand in the experimental girders. As described by the Hoyer effect, radial stress is greatest at the member end and reduces to near zero at the end of the transfer length.

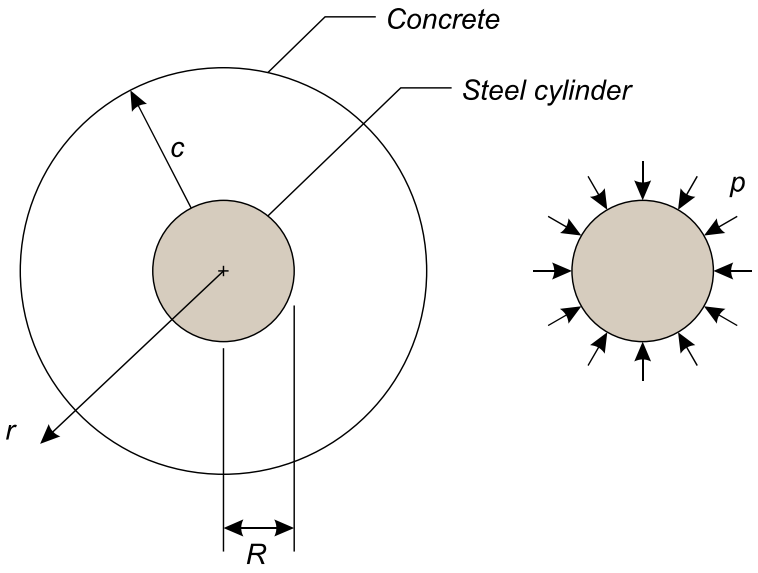

Figure 15–Strand physical analog (based on Oh et al. 2006)

Figure 16–Calculated radial stress (p) distribution (based on Oh et al. 2006)

$$p = \frac{r_0\left(1 - \nu_p f_{pz}/E_p\right) - r_j(1 - \nu_c f_{cz}/E_c)}{\left(1 - \nu_p\right) r_0/E_p + [\nu_c - (r_j^2 + c^2)/(r_j^2 - c^2)]r_j/E_c} \quad \text{2-1}$$

Where:

p = Radial stress at strand-concrete interface
r_o = Strand radius before pretensioning
ν_p = Strand Poisson ratio
f_{pz} = Axial stress in strand

E_p = Strand Elastic Modulus
r_j = Strand radius immediately after pretensioning
ν_c = Concrete Poisson ratio
f_{cz} = Concrete stress in direction parallel to strand
E_c = Concrete Elastic Modulus
c = Concrete cover distance

The equation above assumes linear-elastic behavior. Recognizing the possibility of concrete cracks forming near the strand, the Oh model also includes features to calculate the average stress in cracked concrete. Applying these features results in stresses that are smaller than those calculated by assuming linear-elastic behavior. Cracking features in the Oh model are neglected in the current model development. This approach allows superposition of Hoyer stresses with stresses derived from linear-elastic finite element modeling.

Stress calculated by Equation 2-1 is not sensitive to concrete cover (c) distance for cover values greater than approximately 10 times the strand diameter (Figure 17). By assuming that the cover distance is large relative to the strand diameter, the term $(r_j^2 + c^2)/(r_j^2 - c^2)$ in the denominator of Equation 2-1 approaches negative one, and Equation 11-1 can be simplified to:

$$p = \frac{r_0\left(1 - \nu_p f_{pz}/E_p\right) - r_j(1 - \nu_c f_{cz}/E_c)}{\left(1 - \nu_p\right) r_0/E_p + (\nu_c + 1) r_j/E_c} \qquad 2\text{-}2$$

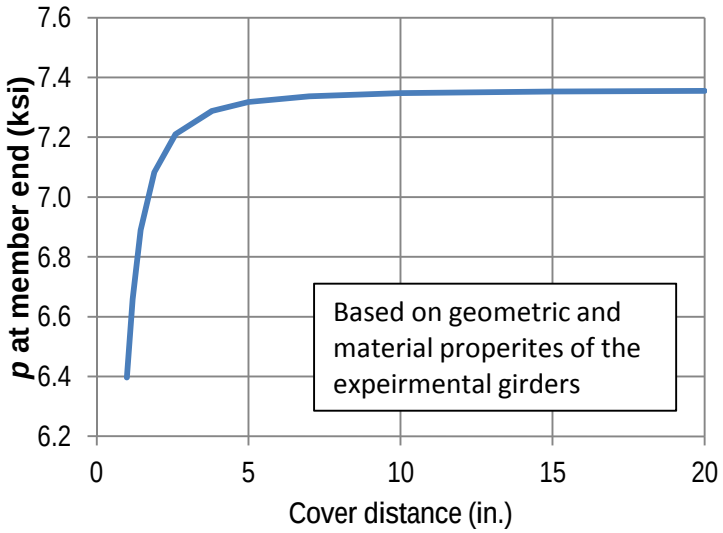

Figure 17–Effect of cover distance on calculated radial stress (p)

Assuming large concrete cover distance is conservative and results in slightly higher calculated stresses. For typical strand diameters and minimum cover dimensions, this assumption increases the calculated stress by less than 2%.

The serviceability model considers stresses at the girder end. At this location, strand expansion and the associated Hoyer stresses are at their maximum. Axial stress in the strand ($f_{pz} = 0$) and concrete ($f_{cz} = 0$) are equal to zero at the member end, which reduces Equation 2-2 to:

$$p_{edge} = \frac{r_0 - r_j}{(1 - \nu_p)\, r_0/E_p + (\nu_c + 1) r_j/E_c} \qquad 2\text{-}3$$

Where:

p_{edge} = Radial stress at strand-concrete interface at end of member

Concrete circumferential stresses are a function of the interfacial stress, strand size, concrete cover, and distance from the strand. Oh et al. provide the following equation for calculating circumferential stresses:

$$\sigma_\theta(r) = \frac{-p\,(1/c^2 + 1/r^2)}{(1/c^2 + 1/R^2)} \qquad 2\text{-}4$$

Where:

σ_θ = Radial stress at strand-concrete interface at end of member
r = Ordinate in the radial direction
R = Radius of prestressing strand

Figure 18 shows the concrete stress distribution calculated by Equations 2-3 and 2-4 for a single strand in the experimental girders. Values used to calculate the stress distribution are listed in Table 1. The maximum concrete stress is 7.35ksi and occurs adjacent to the strand. Stress decreases rapidly with increasing distance from the strand. At locations 2in. from the strand-concrete interface the stress is less than 0.125ksi.

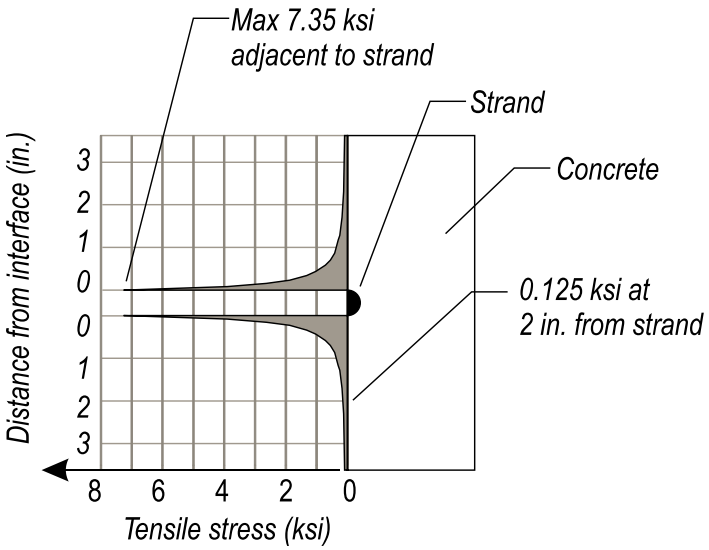

Figure 18–Concrete stress distribution due to Hoyer effect

Table 1–Strand and concrete properties of experimental girders

Concrete Elastic Modulus	4700 ksi
Concrete Poisson Ratio	0.2
Strand Elastic Modulus	29,000 ksi
Strand Poisson Ratio	0.3
Strand radius prior to jacking	0.3 in.
Strand radius after jacking	0.2994 in.

Large Hoyer stress adjacent to strand can cause local damage and cracking in the concrete. If tension through the flange is sufficient, then the localized cracking may propagate and form a crack through the entire flange. For this reason it is important to check the average stress due to the Hoyer effect through the flange thickness.

Rather than calculating average stress from the stress distribution described by Equation 2-4, average stress in the model is calculated indirectly using the interfacial stress. This is done to simplify the design model for design purposes and to avoid integration of concrete stress such as shown in Figure 18. Average stress calculated indirectly from the interfacial stress is the same as average stress calculated by integrating Equation 2-4.

Applying equilibrium to an idealized strand, the interface stress must equal the internal stress in the strand (Figure 19a). Equilibrium can also be applied along a section cut through the strand and concrete (Figure 19b) to show that the resultant force acting on the strand is equal and opposite the concrete force. This equilibrium condition is described by Equation 2-5.

$$\Sigma F_x = 0 = -p d_b d_y + f_{hs}(h_f - d_b) d_y \qquad 2\text{-}5$$

Where:

d_b = Strand diameter
d_y = Differential length in y direction
f_{hs} = Average Hoyer stress on the section from a single strand
h_f = Thickness of flange at section under consideration

Rearranging Equation 2-5, average stress due to the Hoyer Effect can be described as:

$$f_{hs} = \frac{p\, d_b}{(h_f - d_b)} \qquad 2\text{-}6$$

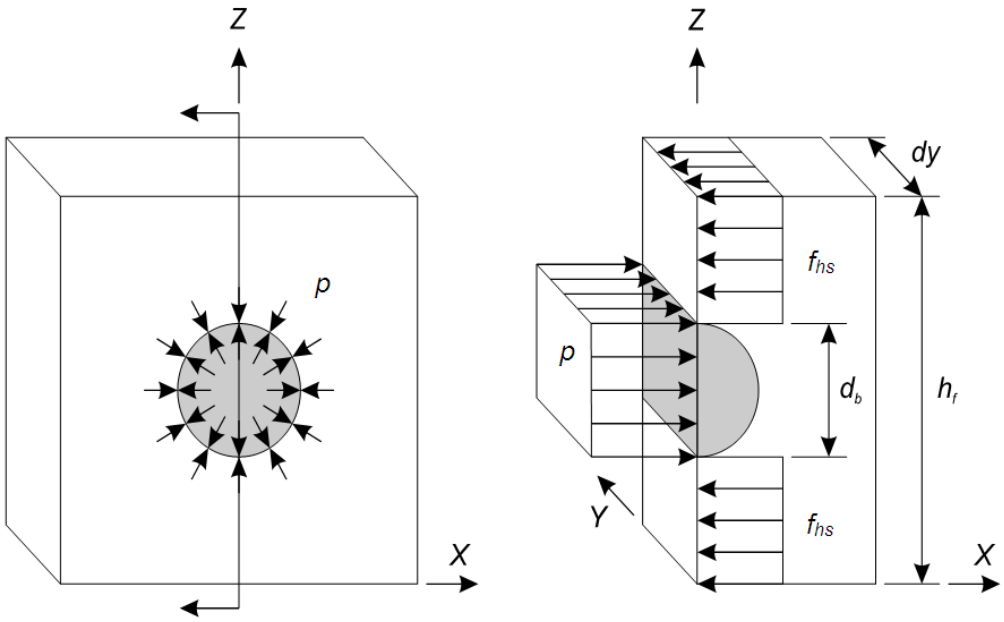

Figure 19–Stresses at plane cut through strand and concrete

The average Hoyer stress on a given line is a function of the quantity of strands on that line. For sections with multiple strands the average stress can be calculated by multiplying the stress from Equation 2-6 by the number of strands. Both shielded and bonded strands along a section displace the area of concrete that carries Hoyer stresses. The denominator in Equation 2-7 is adjusted to account for displaced concrete due to all strands:

$$f_h = \frac{n_s\, p\, d_b}{\left(h_f - n_{st}\, d_b\right)} \qquad 2\text{-}7$$

Where:

f_h = Average stress on the section due to Hoyer Effect
n_s = Quantity of fully bonded strands on section under consideration
n_{st} = Quantity of all strands on section under consideration

The serviceability model considers stress at the end of the member. At this location the interfacial stress between the strand and the concrete can be calculated using Equation 2-3. Substituting Equation 2-3 into Equation 2-7 results in Equation 2-8 for calculating the average Hoyer stress on a line through the bottom flange at the member end:

$$f_h = \frac{n_s\, d_b}{\left(h_f - n_{st} d_b\right)}\left[\frac{r_0 - r_j}{\left(1-\nu_p\right) r_0/E_p + (\nu_c + 1) r_j/E_c}\right] \qquad 2\text{-}8$$

G.2.2.2 Peeling Stress

Peeling stress calculations are based on the free body diagram shown in Figure 20. This diagram is a simplified illustration of forces acting on the outer portion on a bottom flange during prestress transfer. Prestressing forces from the eccentric outer strands (F_{pos}) create a moment about the Z-axis. Moment equilibrium is maintained by x-direction tensile stresses in the concrete acting on the Y-Z cut plane. This equilibrium condition is described in equation 2-9:

$$\Sigma M_Z = 0 = F_{pos} x_p - F_{tos} l_y \qquad 2\text{-}9$$

Where:

F_{pos} = Prestressing force from strands outboard of cut plane
x_p = Distance from cut plane to centroid of prestressing force
F_{tos} = Transverse tension force acting on cut plane due to eccentric prestressing
l_y = Internal moment arm in y-direction

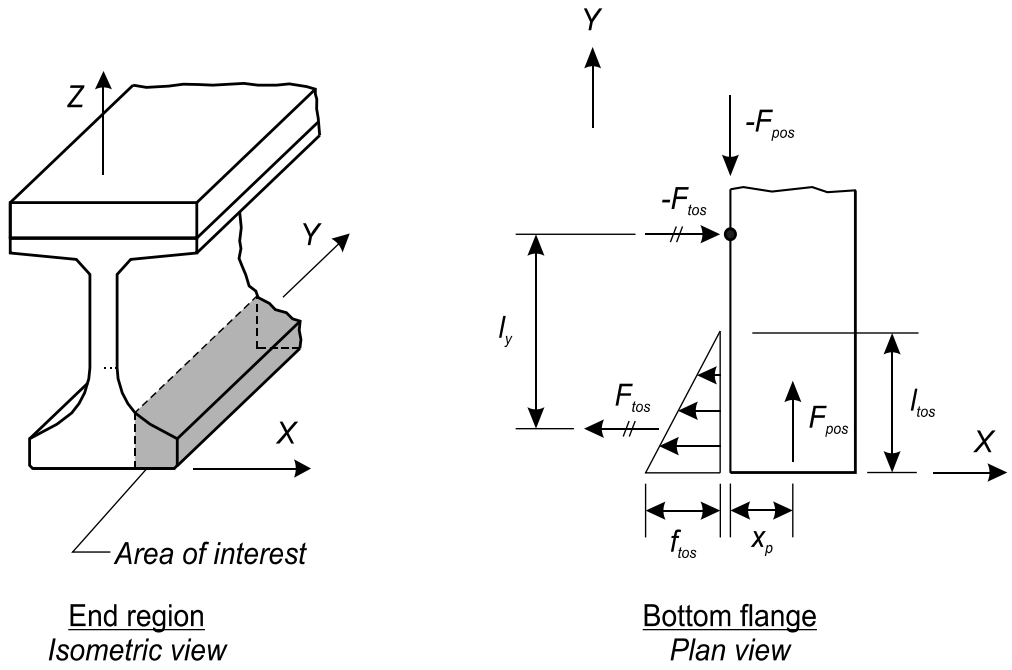

Figure 20–Bottom flange free body diagram

Rearranging Equation 2-9 results in the following equation for the transverse tension force due to the eccentric strands:

$$F_{tos} = \frac{F_{pos} x_p}{l_y} \qquad 2\text{-}10$$

Transverse tensile force in Equation 2-10 is the resultant of peeling stress in the concrete at the member end, which is assumed to have a triangular tensile stress distribution. Peeling stress is assumed to be largest at the member end and zero at a distance l_{tos} from the end (Figure 20). Previous FE modeling shows that a triangular stress distribution and a value of 10in. for l_{tos} are reasonable assumptions cross-sections with outer strands cut (See Appendix F). The following equation of equilibrium ensures that the resultant force from the assumed peeling stress distribution is equal the transverse tensile force:

$$F_{tos} = \frac{F_{pos} x_p}{l_y} = \frac{1}{2} f_{tos} l_{tos} h_f \qquad 2\text{-}11$$

Where:

f_{tos} = Peeling stress
l_{tos} = Length of the assumed tensile stress distribution

h_f = Thickness of the flange at the section under consideration

Equation 2-11 can be rearranged to solve for the peeling stress at the member end:

$$f_{tos} = \frac{2F_{pos}x_p}{l_y l_{tos} h_f} \quad \text{2-12}$$

Strands along a given section displace the concrete area that carries peeling stress. The denominator in Equation 2-12 must be adjusted to account for the area displaced by shielded and bonded strands. Doing so results in:

$$f_{tos} = \frac{2F_{pos}x_p}{l_y l_{tos}(h_f - n_{st}d_b)} \quad \text{2-13}$$

The term l_y in Equation 2-13 is the length of the internal moment arm in the y-direction. The value of l_y varies according to the quantity of cut strands, shape of the cross-section, and location within a given cross-section. Equation 2-14 and 2-15 are empirical equations for calculating l_y in FIB girders. These equations were found to give values of l_y -and consequently of F_{tos}- that are in agreement with previous FE results.

$$l_{y1} = 36\frac{\sqrt{h_f}}{\sqrt{x}} \quad \text{2-14}$$

$$l_{y2} = 53\frac{h_f}{x} \quad \text{2-15}$$

Where:

l_{y1} = Internal moment arm in the y-direction for maximum peeling condition
l_{y2} = Internal moment arm in the y-direction for combined condition
h_f = Thickness (z-dimension) of the flange at the section under consideration
x = x-ordinate of the section under consideration

Transverse forces calculated using Equation 2-13 and Equation 2-14 or Equation 2-15 are compared with previous FE results (see appendix F) in Table 2 and Table 3. Results are compared for the MID and EDGE sections (Figure 21), for the 'design' strand bond pattern used in the FIB-54 experimental program. Values from the model equations are within 1% of FE results for all but the combined condition at the MID section, for which the model is 7%

conservative. Consistency between the model and FE results indicates that Equations 2-14 and 2-15 are acceptable approximations for calculating l_y in FIB girders.

Table 2–Model vs. FE for maximum peeling stress condition

Section	h_f (in.)	x (in.)	l_{y1} (in.)	F_{tos} Model (kip)	F_{tos} FE (kip)	Model / FE
EDGE	10.5	12	46.4	11.4	11.3	1.01
MID	12.9	8	85.5	20.6	20.3	1.01

Table 3–Model vs. FE for combined stress condition

Section	h_f (in.)	x (in.)	l_{y2} (in.)	F_{tos} Model (kip)	F_{tos} FE (kip)	Model / FE
EDGE	10.5	12	33.7	15.7	15.9	0.99
MID	12.9	8	45.7	38.5	36.1	1.07

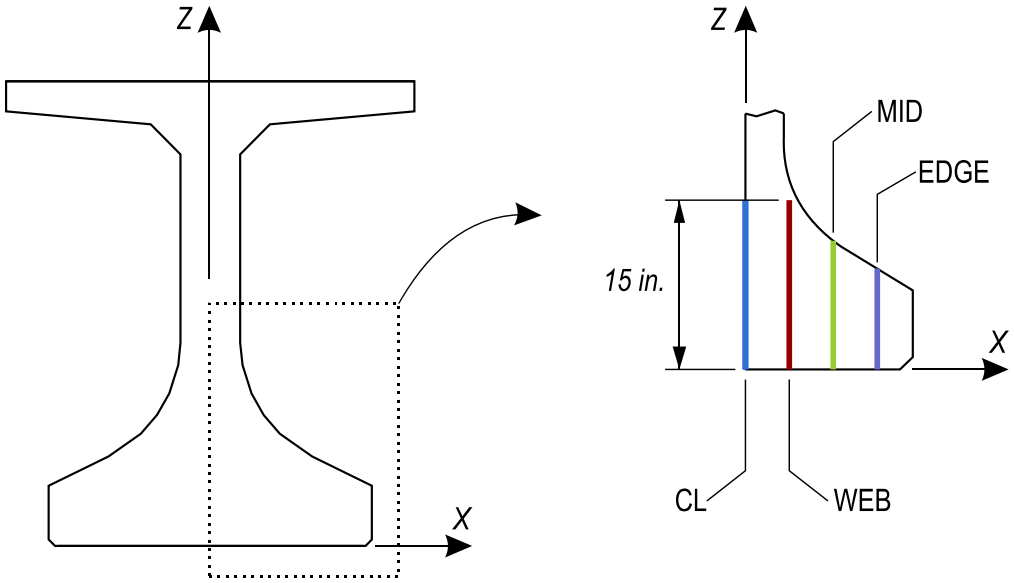

Figure 21–Analysis locations for determining F_{tos}

Equations 2-14 and 2-15 are empirically derived for FIB girders and are assumed reasonable for any girder with a similar flange aspect ratio. Different equations are needed for calculating l_y in girders with relatively stocky flanges, such as AASHTO girders. Equations 2-16 and 2-17 are for use with relatively stocky girders. These equations are empirically derived by comparison with previous FE results. Figure 22 shows the FE mesh, strand locations, and bottom flange sections used for the comparison. See appendix F for additional information on

the FE modeling. Transverse forces calculated using Equation 2-13 and Equations 2-16 or 2-17 are compared with FE results in Table 4 and Table 5. At the FLANGE section, the design model results in transverse forces that are within 1% of the FE results. The model is more conservative at the WEB section, resulting in values that are 7% to 9% larger than the FE model. Based on these favorable comparisons, Equations 2-16 and 2-17 are considered acceptable approximations for calculating l_y in AASHTO girders and other girders with stocky flanges.

$$l_{y1} = 19\frac{h_f}{x} \qquad 2\text{-}16$$

$$l_{y2} = 1.85\frac{h_f^2}{x} \qquad 2\text{-}17$$

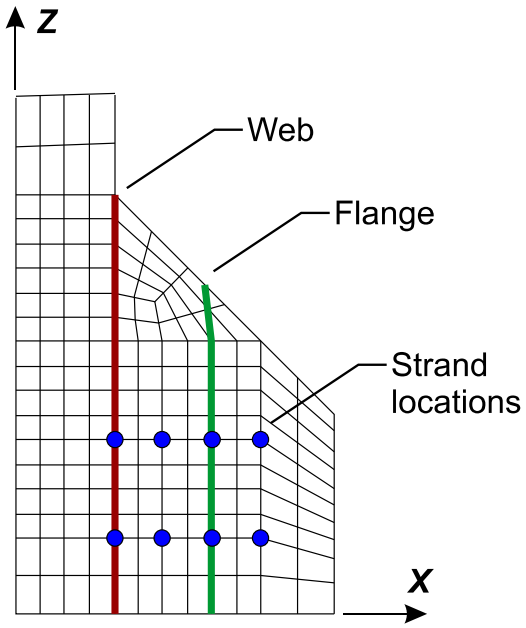

Figure 22–AASHTO girder FE model and analysis locations

Table 4–Model vs. FE for maximum peeling stress condition

Section	h_f (in.)	x (in.)	l_{y1} (in.)	F_{tos} Model (kip)	F_{tos} FE (kip)	Model / FE
WEB	17	4	80.8	12.4	11.4	1.09
FLANGE	12	8	28.5	5.0	5.9	1.00

Table 5–Model vs. FE for combined stress condition

Section	h_f (in.)	x (in.)	l_{y2} (in.)	F_{tos} Model (kip)	F_{tos} FE (kip)	Model / FE
WEB	17	4	133.7	7.5	7.0	1.07
FLANGE	12	8	33.3	5.0	5.0	1.00

Substituting l_{y1} and l_{y2} in into Equation 2-13 results in Equations 2-18 and 2-19. These equations are calibrated for sections through the outer portion of the bottom flange in FIB girders. They should not be used in conjunction with other girder shapes, or at sections in the FIB bottom flange that are below the web.

$$f_{tos1} = \frac{2F_{pos}x_p}{l_{y1}l_{tos}(h_f - n_{st}d_b)} \quad \text{2-18}$$

$$f_{tos2} = \frac{2F_{pos}x_p}{l_{y2}l_{tos}(h_f - n_{st}d_b)} \quad \text{2-19}$$

G.2.2.3 Self-Weight Reaction Stress

Analytical modeling has shown that self-weight reaction stress at the end surface of FIB girders can be neglected at locations in the outer portion of the bottom flange. As such, the self-weight reaction stress (f_{sw}) in the serviceability model is assumed to be zero. This assumption may not be reasonable for all cross-sections.

G.2.2.4 Superposition of Stresses

Horizontal spitting stress is defined as the superposition of Hoyer, peeling, and self-weight reaction stresses:

$$f_{hsp} = f_h + f_{tos} + f_{sw} \quad \text{2-20}$$

Where:

f_{hsp}= Horizontal splitting stress
f_h= Average Hoyer effect stress
f_{tos}= Peeling stress
f_{sw}= Self-weight reaction stress

As previously discussed, stress due to self-weight reaction is negligible at the end face of the FIB bottom flange. Self-weight reaction is included in Equation 2-20 only as a reminder that self-weight effects may be critical in some long-span girders and in girders with other cross-sections. For FIB girders, Equation 2-20 can be reduced to:

$$f_{hsp} = f_h + f_{tos} \quad \text{2-21}$$

Two critical conditions have been discussed for horizontal splitting stresses. The maximum peeling condition occurs when only the strands outboard of a section are cut. Strands at the section in question are not yet cut in the maximum peeling condition and Hoyer stress on the section is assumed to be zero. The combined condition occurs when strands on a section have been cut and peeling stress is superimposed with Hoyer stress. The maximum horizontal splitting stress on a given section is the greater of the stress from the maximum peeling or combined conditions:

$$f_{hsp1} = f_{tos1} \quad \text{2-22}$$

$$f_{hsp2} = f_h + f_{tos2} \quad \text{2-23}$$

Where:

f_{hsp1}= Horizontal splitting stress for maximum peeling condition
f_{hsp2}= Horizontal splitting stress for combined condition

In FIB girders transverse splitting stresses is checked for the five outermost columns of strands (Figure 23). Stresses are checked at strand locations because Hoyer stresses are greatest near prestressing strands, and because splitting cracks in the experimental program were observed to intersect strands. Stress is checked at each of the five locations for both of the critical stress conditions. Maximum stress from these locations and conditions is compared to concrete tensile strength criterion, which is discussed later.

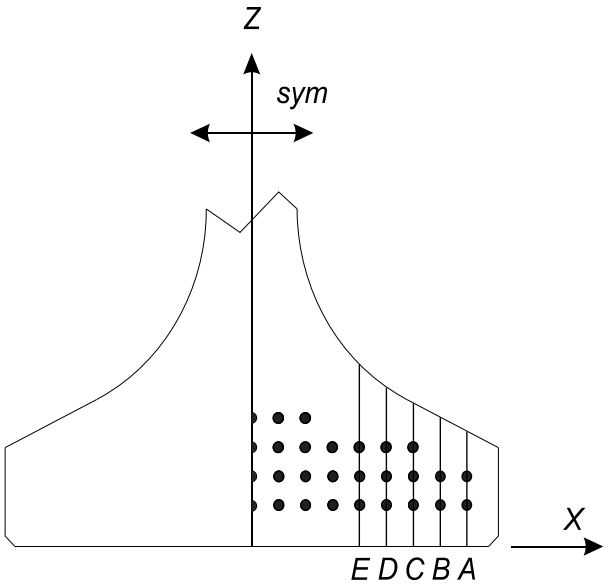

Figure 23–Analysis sections for FIB bottom flange

G.2.3 Stress Calculations for Experimental Girders

In this section the serviceability model is used to compute stresses at the end of specimen WN (Figure 24). The end of specimen WN had two fully bonded strands placed at the outside of the flange. All other strands in the outer flange were shielded.

Hoyer stresses were calculated using Equation 2-8 and are summarized in Table 6. The value of interfacial pressure (p) listed in Table 6 was calculated using Equation 2-3 and the values from Table 1. The calculated Hoyer stress is zero for all but section A. This is because the model assumes that Hoyer stresses from shielded strands are negligible.

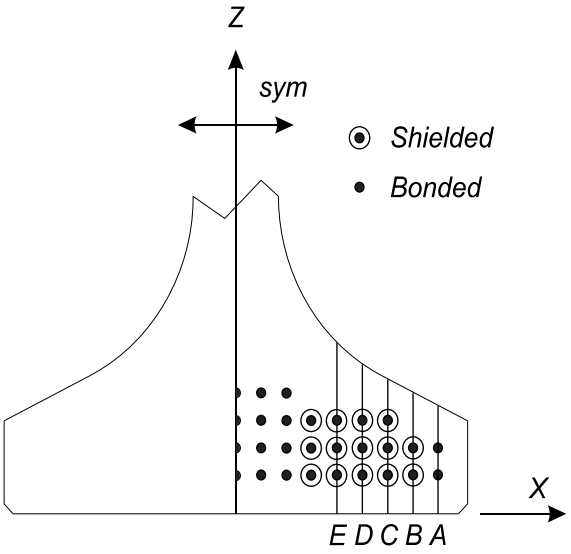

Figure 24–Strand bond and shielding pattern specimen WN

Table 6–Hoyer stresses end of specimen WN

Section	n_s	p (ksi)	d_b (in.)	n_{st}	h_f (in.)	f_h (ksi)
A	2	7.36	0.6	2	8.5	1.21
B	0	7.36	0.6	2	8.5	0
C (EDGE)	0	7.36	0.6	3	8.5	0
D	0	7.36	0.6	3	8.5	0
E (MID)	0	7.36	0.6	3	8.5	0

Peeling stresses were calculated using Equations 2-18 and 2-19 and are summarized in Table 7. Peeling stresses at section B require additional discussion. The maximum peeling condition is intended to have the maximum peeling stress, however, it has a lower peeling stress than the combined condition at section B. This is because empirical equations for the internal moment arm resulted in a shorter arm, and consequently at larger peeling stress, for the combined condition. This limitation of the model only affects section B and is of little concern. As shown later in the chapter, splitting stress at section B does not govern in any of the stress calculations for the experimental specimens. Also, this limitation makes the model is conservative at section B because it superimposes the larger peeling stress with the Hoyer stress.

Horizontal splitting stresses were calculated using Equations 2-22 and 2-23 and the stresses from Table 6 and Table 7. Results are presented graphically in Figure 25. The maximum calculated splitting stress at the end of WN occurs at section A during the combined condition. Because no peeling stress occurred at section A, the entire calculated splitting stress is due to the Hoyer effect. Splitting stresses at the other sections in WN are smaller than at section A because Hoyer stress from the shielded strands is assumed to be negligible. Calculated splitting stresses at sections B through E are solely due to peeling stresses caused by the bonded strands at section A.

Table 7–Peeling stresses at end of specimen WN

Section	F_{pos} (kip)	x_p (in.)	x (in.)	h_f (in.)	n_{st}	d_b (in.)	l_{y1} (in.)	l_{y2} (in.)	f_{tos1} (ksi)	f_{tos2} (ksi)
A	NA	NA	16	8.5	2	0.6	NA	NA	0	0
B	88	2	14	9.5	2	0.6	43.7	36.0	0.097	0.118
C (EDGE)	88	4	12	10.4	3	0.6	38.7	45.9	0.212	0.178
D	88	6	10	11.6	3	0.6	33.4	61.5	0.322	0.175
E (MID)	88	8	8	13.2	3	0.6	28.0	87.5	0.441	0.141

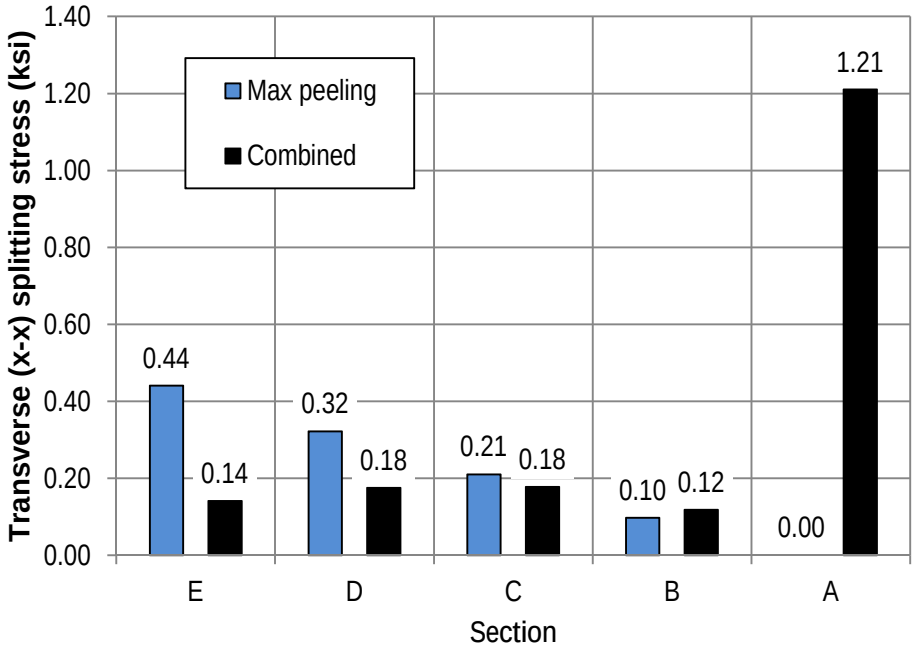

Figure 25–Transverse (x-x) splitting stress at end of specimen WN

The same procedures used above for WN were also used calculate transverse splitting stresses for each specimen in the FIB-54 and FIB-63 experimental programs. The serviceability model was derived for calculating stresses at the end of pretensioned I-girders. To test the applicability of the model to other locations, it was also used to estimate stress in specimens WN, WB, and SL where shielding terminated.

The maximum transverse splitting stress for each specimen and location are listed in Table 8, along with the governing section, governing stress condition, and flange splitting crack data. When stresses were calculated at two locations on the same specimen, crack data were assigned to the location where the cracks were observed in the physical girder. For example, no splitting cracks were observed at the end of specimen WN and the table lists zero for the crack length and area. Splitting cracks were observed 10 ft away from the end of WN, and the table lists the length and area of those cracks in the row labeled “WN (10 ft.)”.

Table 8–Transverse splitting stresses and splitting crack data

Specimen	Max transverse splitting stress (ksi)	Section	Critical Condition	Length of flange splitting cracks (in.)	Area of flange splitting cracks (in^2)
HC	1.29	C	Combined	0	0
HU	1.29	C	Combined	40	0.112
VC	1.29	C	Combined	0	0
VU	1.29	C	Combined	41	0.087
WN (10 ft.)	1.63	C	Combined	32	0.05
WB (10 ft.)	1.63	C	Combined	99	0.292
WN (end)	1.21	A	Combined	0	0
WB (end)	1.21	A	Combined	0	0
FN	1.73	D	Combined	190	0.469
FB	1.73	D	Combined	115	0.295
DC	1.29	C	Combined	104	0.239
DM	1.29	C	Combined	41.5	0.112
PT	1.81	C	Combined	142	0.316
LB	1.81	C	Combined	183	0.429
CN	1.81	C	Combined	175	0.368
SL	1.25	C	Combined	73	0.144
SL (5 ft.)	0.99	D	Combined	0	0

Table 8 shows that the combined stress condition governs for each specimen and location. For the combined condition Hoyer stress accounted for 85% of the splitting stress, on average. The remaining 15% (on average) was from peeling stress. This result indicates the significance that the Hoyer effect has on flange splitting cracks.

Section C has the governing (maximum) stress in 12 of 17 specimens and locations. Experimental observations support this result. Flange splitting cracks were more likely to be observed at section C than at any other location in the experimental program. The governing stress from the model never occurs at sections B or E. This result supports the previous statement that model limitations at section B do not impact overall results.

G.2.4 Model Comparison with Experimental Crack Data

Stresses calculated using the serviceability model correlate well with crack data from the experimental girders (Table 8 and Figure 26). This can be seen from the linear curve in Figure 26 that is fit to the stress and crack data from the specimen ends. The line has an R^2 value of 0.85, indicating a high degree of correlation between calculated stresses and experimental crack lengths. When stress and crack data away from the ends (WN, WB, and SL) are included,

correlation drops to 0.73. This suggests that the model is more accurate for calculating stress at member ends than at sections away from the end. Additional data are required, however, to quantify the degree to which the model can reasonably be applied to locations away from the member end.

A high degree of correlation is also observed when the calculated stresses are compared to the area of the flange splitting cracks in the experimental girders (Figure 27). Considering the random nature of cracking in concrete this level of correlation suggests that the model does an excellent job of capturing the physical phenomenon which cause bottom flange splitting cracks.

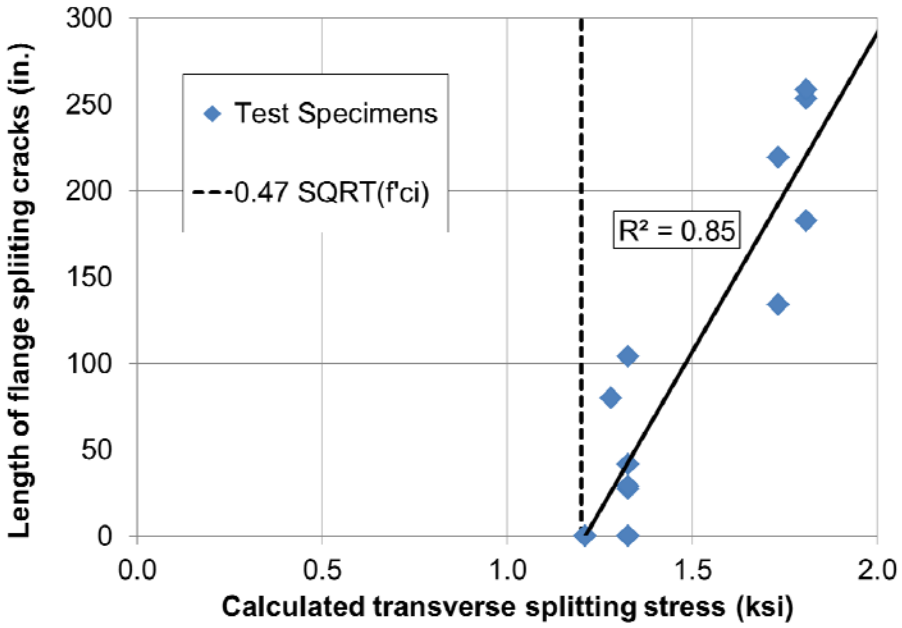

Figure 26–Calculated transverse splitting stress vs. experimental crack length

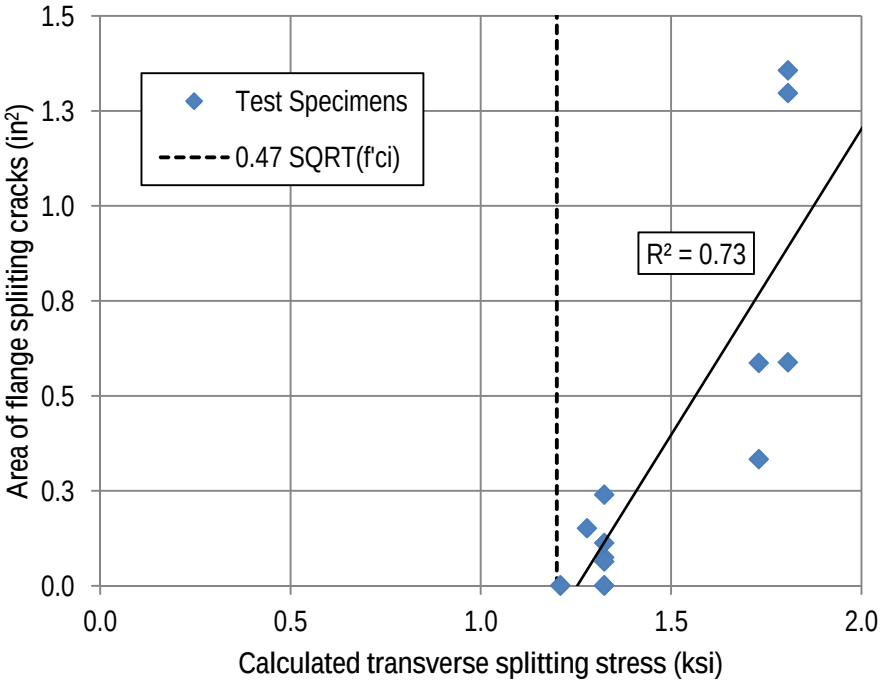

Figure 27–Calculated transverse splitting stress vs. experimental crack area

It is common in prestressed concrete design to compare concrete tensile stress to the square root of the compressive strength. Dashed vertical lines in Figure 26 and Figure 27 indicate 1.20ksi which is equal to $0.47\sqrt{f'_{ci}}$ (for f'_{ci} in ksi). This value is approximately equal to the x-intercept of the linear curves fit to the data. The x-intercept corresponds to the stress below which flange cracking are unlikely according to the sample data. All but one of the specimens and locations in the sample have stresses higher than this value. The lone location below this value, SL (5ft.), did not have flange splitting cracks in the experimental girder. A more conservative stress limit, and one that is already used in other circumstances by AASHTO LRFD, is $0.24\sqrt{f'_{ci}}$. This is approximately half of the limit indicated by the experimental data. Additional data are required to calibrate the reliability associated with different splitting stress criteria. Nevertheless, available data suggest that the proposed model is an adequate tool for calculating transverse splitting stress in the bottom flange of FIB girders.

G.2.5 Summary and Conclusions

A model was derived for calculating transverse splitting stresses in the bottom flange of concrete I-girders. The model considers contributions to splitting stress from the Hoyer effect

and from the horizontal eccentricity of strands in the outer flange. Stresses due to these effects are referred to as Hoyer stresses and peeling stresses, respectively. Self-weight also contributes to transverse splitting stress, however effects of self-weight are considered negligible in the outer flange. The work of Oh et al (2006) was utilized to derive an equation for Hoyer stress. An equation for peeling stress was derived using FE modeling and basic mechanics. The equation for peeling stress also contains empirical relationships that were derived by comparison with FE analyses.

The model was compared to crack data from the experimental girders and was found to have a high degree of correlation with said data. An R^2 value of 0.80 was obtained for linear trend line that was fit to the calculated and experimental data. Analysis indicates that flange splitting cracks are likely when the calculated splitting stress exceeds $0.45\sqrt{f'_{ci}}$ (for f'_{ci} in ksi). A lower threshold stress is recommended for controlling flange splitting cracks. One possible threshold is $0.24\sqrt{f'_{ci}}$, which is currently used by AASHTO LRFD to limit concrete tensile stresses in situations similar to the FIB bottom flange.